

Article

Study of High-Energy Proton Irradiation Effects in Top-Gate Graphene Field-Effect Transistors

Xiaojie Lu ^{1,2}, Hongxia Guo ^{1,3,*}, Zhifeng Lei ², Chao Peng ², Zhangang Zhang ², Hong Zhang ², Teng Ma ², Yahui Feng ³, Wuying Ma ³, Xiangli Zhong ¹, Jifang Li ¹, Yangfan Li ¹ and Ruxue Bai ¹

- ¹ School of Material Science and Engineering, Xiangtan University, Xiangtan 411105, China; 202121551427@smail.xtu.edu.cn (X.L.); xlzhong@xtu.edu.cn (X.Z.); 202121551403@smail.xtu.edu.cn (J.L.); 202121551519@smail.xtu.edu.cn (Y.L.); 202331550182@smail.xtu.edu.cn (R.B.)
- ² Science and Technology on Reliability Physics and Application of Electronic Component Laboratory, China Electronic Product Reliability and Environmental Testing Research Institute, Guangzhou 510610, China; leizhifeng@ceprei.com (Z.L.); pengchao@ceprei.com (C.P.); zhangzhangang@ceprei.com (Z.Z.); 201931000121@smail.xtu.edu.cn (H.Z.); mateng@ceprei.com (T.M.)
- ³ Northwest Institute of Nuclear Technology, Xi'an 710024, China; 22111110506@stu.xidian.edu.cn (Y.F.); mawuying@nint.ac.cn (W.M.)
- * Correspondence: guohongxia@nint.ac.cn

Abstract: In this article, the effects of high-energy proton irradiation on top-gate graphene field-effect transistors (GFETs) were investigated by using 20 MeV protons. The basic electrical parameters of the top-gate GFETs were measured before and after proton irradiation with a fluence of 1×10^{11} p/cm² and 5×10^{11} p/cm², respectively. Decreased saturation current, increased Dirac sheet resistance, and negative drift in the Dirac voltage in response to proton irradiation were observed. According to the transfer characteristic curves, it was found that the carrier mobility was reduced after proton irradiation. The analysis suggests that proton irradiation generates a large net positive charge in the gate oxide layer, which induces a negative drift in the Dirac voltage. Introducing defects and increased impurities at the gate oxide/graphene interface after proton irradiation resulted in enhanced Coulomb scattering and reduced mobility of the carriers, which in turn affects the Dirac sheet resistance and saturation current. After annealing at room temperature, the electrical characteristics of the devices were partially restored. The results of the technical computer-aided design (TCAD) simulation indicate that the reduction in carrier mobility is the main reason for the degradation of the electrical performance of the device. Monte Carlo simulations were conducted to determine the ionization and nonionization energy losses induced by proton incidence in top-gate GFET devices. The simulation data show that the ionization energy loss is the primary cause of the degradation of the electrical performance.

Keywords: top-gate graphene field-effect transistors (GFETs); 20 MeV proton irradiation; technical computer-aided design (TCAD); ionization energy loss



Citation: Lu, X.; Guo, H.; Lei, Z.; Peng, C.; Zhang, Z.; Zhang, H.; Ma, T.; Feng, Y.; Ma, W.; Zhong, X.; et al. Study of High-Energy Proton Irradiation Effects in Top-Gate Graphene Field-Effect Transistors. *Electronics* **2023**, *12*, 4837. <https://doi.org/10.3390/electronics12234837>

Academic Editor: Frédérique Ducroquet

Received: 1 November 2023

Revised: 24 November 2023

Accepted: 28 November 2023

Published: 30 November 2023



Copyright: © 2023 by the authors. Licensee MDPI, Basel, Switzerland. This article is an open access article distributed under the terms and conditions of the Creative Commons Attribution (CC BY) license (<https://creativecommons.org/licenses/by/4.0/>).

1. Introduction

The study of irradiation effects on semiconductors and electronic devices has received increasing attention over the past few years. The study of the effect that irradiation has on different materials, such as organics and metal oxides, has also received increasing attention [1–3]. Since graphene was first exfoliated from bulk graphite in 2004 [4], it has been found that graphene has the advantages of single-atom thickness, ultra-high carrier mobility, and high thermal conductivity, which can improve the electrical performance of semiconductor devices and reduce the short-channel effect of transistors [4–8]. The fact that graphene material is only a single-atomic-layer thick and lacks a bulk crystal structure gives graphene good resistance to radiation [9], making it promising for applications in the space field. Based on studies of the effects of proton irradiation on other aerospace

devices [10–12], the total ionizing dose (TID) and displacement damage effects significantly impact the electrical performance of aerospace devices. Studying the total ionizing dose (TID) and displacement damage effects caused by proton irradiation on graphene field-effect transistors is essential. The result of proton radiation on top-gate graphene field-effect transistors (GFETs) should not be overlooked because it is the predominant component of solar and galactic cosmic rays. Some research has been performed on the impacts of irradiation damage on GFET devices and graphene materials. G. Ko et al. [13] irradiated few-layer graphene samples with five MeV protons. The investigation demonstrates that proton irradiation leads to an increase in the surface state of graphene and a significant decrease in hole mobility and resistance. Yang G. et al. [14] irradiated monolayer graphene with 5–15 MeV protons and analyzed it using microscopic Raman spectroscopy. The results show that the electrical properties of graphene change from bipolar to P-type as the degree of disorder increases. Cui N. et al. [15] irradiated GFETs with electrons and protons at 40 keV. The research indicates that irradiation leads to graphene lattice damage in which the effective scattering of protons and/or the damage cross-section is substantially larger. Francis S. A. et al. [16] irradiated back-gate GFETs with 10 keV X-rays and 1.8 MeV protons. The data reveal that oxygen doping due to X-ray irradiation increases the drain current and that dedoping and displacement damage produced by protons leads to an instantaneous drop in the drain current. Zhang Y. et al. [17] irradiated GFETs with three MeV protons. The results show that the irradiation leads to charge accumulation at the graphene/SiO₂ interface, where the graphene exchanges charge with the adsorbed particles, compounding the accumulated charge. Studies on the effect of γ -rays on graphene devices have shown that irradiation creates defects at the graphene/oxide interface and in the bulk oxide, promotes the adsorption of oxygen in graphene, and leads to a decrease in carrier mobility and an increase in the doping concentration, resulting in a change in sheet resistance [18,19]. Experimental studies have shown that protons of different energies produce different defects, leading to different irradiation effects [20]. However, today's studies on the radiation effects in GFET devices mainly focus on the low-energy proton. In this article, the radiation effect of high-energy protons on GFET devices is investigated to investigate the damage mechanism of the device further.

In this article, the irradiation experiments of top-gate GFETs are carried out by employing 20 MeV protons with a fluence of 1×10^{11} p/cm² and 5×10^{11} p/cm². The effects of high-energy proton irradiation on the electrical properties of the device are mainly investigated. Technical computer-aided design (TCAD) tools were used to simulate the effect of carrier concentrations and carrier mobility variations on the transfer characteristic curves of top-gate GFETs. Monte Carlo simulation software was used to simulate ionizing and nonionizing energy losses due to proton injection into top-gate GFETs.

2. Materials and Methods

The sample selected in this experiment was a top-gate GFET device, the channel of which was composed of graphene. The physical diagram of the device is shown in Figure 1. The top-gate GFET device was produced by Graphenea [21]. Graphene was transferred onto a SiO₂/Si substrate by chemical vapor deposition (CVD). The graphene channel length and width were also 50 μ m. The substrate was made of silicon with 90 nm SiO₂ on a 525 μ m silicon substrate. The schematic cross-sectional structure of the top-gate GFET and the schematic channel structure are shown in Figure 2.

The carrier concentration and carrier type (electron or hole) in the channel are determined by the potential difference between the channel and the gate (top-gate and/or back-gate). A large positive gate voltage promotes electron accumulation in the channel (N-type channel), and a large negative gate voltage promotes hole accumulation in the channel (P-type channel). The source–drain current of the top-gate GFETs is bipolar to the gate voltage [22], with two branches of transfer characteristics separated by the Dirac point (the point of minimum drain current on the transfer characteristic curve).

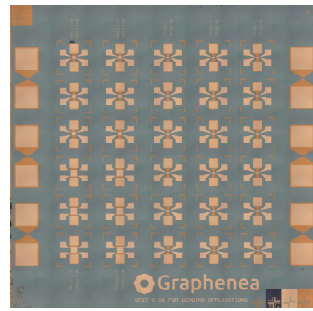


Figure 1. Physical diagram of top-gate GFETs.

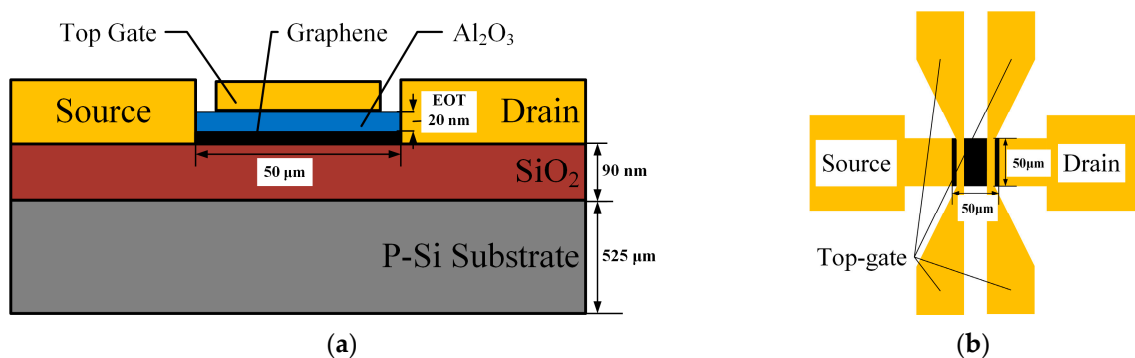


Figure 2. Top-gate GFET structure schematic. (a) Schematic of cross-section structure; (b) Schematic of channel structure.

The proton irradiation of a top-gate GFET device was carried out at the Xi'an 200 MeV proton application facility (XiPAF), which induced a quasi-monoenergetic proton beam of 20 MeV. The irradiation was stopped when the proton fluence reached 1×10^{11} p/cm² and 5×10^{11} p/cm². The fluence rate was 5×10^7 p/cm² s. The size of the chip was 1 cm × 1 cm, and the beam size was 3 cm × 3 cm to make the radiation source enough to irradiate the whole chip uniformly. The device was not yet encapsulated, and the three electrodes of the device floated during irradiation.

3. Results and Discussion

The electrical characteristics of top-gate GFET devices were tested. It was found that the electrical characteristics of the devices decayed to different degrees at different fluences, and the reasons for the decay of the electrical characteristics were analyzed. The effect of graphene channel parameter variations on the electrical characteristics of top-gate GFET devices was investigated using TCAD simulation software. The magnitude and distribution of ionizing and nonionizing energy losses produced by proton irradiation in top-gate GFET devices were analyzed using Monte Carlo simulation software. The effect of proton irradiation on top-gate GFETs was further verified.

3.1. Effect of Proton Irradiation on the Electrical Characteristics of Top-Gate GFETs at Different Fluences

The electrical characteristics of samples before and after proton irradiation and at room-temperature annealing were measured offline using an Agilent B1500A semiconductor parameter analyzer (Agilent, Santa Clara, CA, USA). The electrical characteristics of the top-gate GFET devices were found to be significantly degraded after proton irradiation and partially recovered after annealing. The transfer characteristic curves before and after irradiation and annealing, as well as the graphene channel sheet resistance R_S versus the top-gate voltage, are shown in Figure 3.

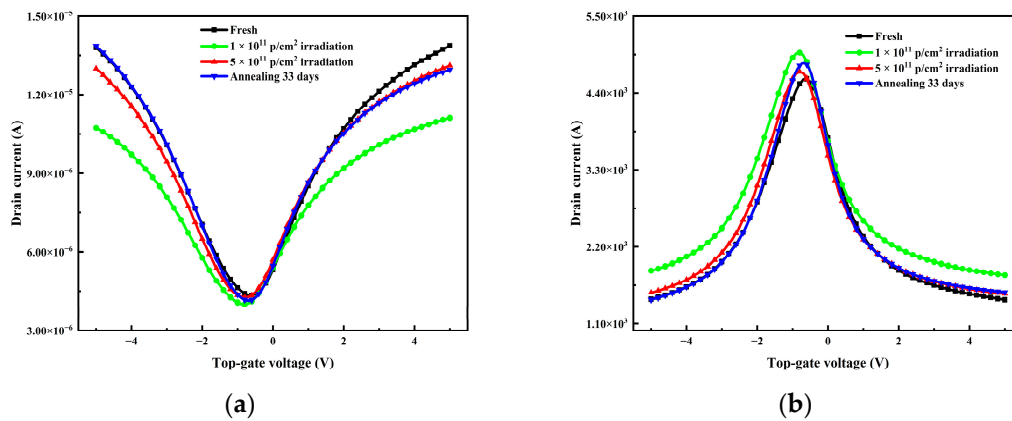


Figure 3. The pre- and postirradiation fluence reached 1×10^{11} p/cm² and 5×10^{11} p/cm², respectively. After annealing at room temperature for 33 days. (a) Transfer characteristic curves. (b) Graphene channel sheet resistance R_S versus top-gate voltage curves.

During the test, the source was grounded, and the drain–source voltage, V_{DS} , was set to 0.02 V, while the gate–source voltage, V_{GS} , ranged from -5.0 V to $+5.0$ V. As shown in Figure 3a, after irradiating the top-gate GFET device with a fluence of 1×10^{11} p/cm² and 5×10^{11} p/cm², the voltages at the Dirac point of the device drifted negatively, both from -0.6 V to -0.8 V. The saturation current of the device was reduced after irradiation, and the decay trend varied with different fluences. After annealing at room temperature for 33 days, the saturation current for hole conduction on the left side of the Dirac voltage was largely restored, while the saturation current for electron conduction on the right side of the Dirac voltage remained essentially unchanged. The Dirac voltage returned to -0.7 V.

The analysis suggests that high-energy proton radiation deposits energy within the gate oxide layer and produces electron–hole pairs. Because the mobility of holes in the gate oxide is much smaller than that of the electrons, most of the holes are trapped in impurity and defect sites at the graphene/gate oxide interface and/or in the gate oxide itself. The generated holes alter the gate voltage and modulate the graphene charge-carrier concentration [23,24], resulting in a negative voltage drift at the Dirac point.

For the transfer characteristics measured in the linear region, the mobility of the carriers (hole and electron) can be derived by Equation (1) [25]:

$$\mu = \frac{\Delta I_{DS}}{C_{ox} \frac{W}{L} V_{DS} \Delta V_{GS}}. \quad (1)$$

where μ is the carrier mobility, W and L are the width and length of the channel, respectively, and C_{ox} is the gate oxide capacitance. The hole and electron mobility extracted by Equation (1) are shown in Table 1.

Table 1. Electron mobility μ_n and hole mobility μ_p for different fluences of proton irradiation and annealing.

Fluence (p/cm ²)	Electron Mobility μ_n (cm ² /Vs)	Hole Mobility μ_p (cm ² /Vs)
0	986.70	926.40
1×10^{11}	801.80 (reduces 18.74%)	709.40 (reduces 23.42%)
5×10^{11}	951.76 (reduces 3.54%)	904.70 (reduces 2.34%)
annealing	980.30 (reduces 0.65%)	907.30 (reduces 2.06%)

The results show that the decreasing saturation current in the transfer characteristic curve follows the trend of decreasing carrier mobility. To better analyze the effects of carrier concentration and carrier mobility on the electrical properties of graphene devices, the variation in sheet resistance at the Dirac point was analyzed. It is known from Equation (2) that

the sheet resistance is related to both carrier concentration and carrier mobility. As shown in Figure 3b, after proton irradiation, the resistance at the Dirac point of the device increases from 4600.45 $\Omega/\text{sq.}$ to 4977.85 $\Omega/\text{sq.}$ (the fluence is 1×10^{11} p/cm²) and 4697.92 $\Omega/\text{sq.}$ (the fluence is 5×10^{11} p/cm²), which is an increase of about 8.20% and 2.12%, respectively. The sheet resistance was 4822.53 $\Omega/\text{sq.}$ after annealing at room temperature.

The value of sheet resistance R_S can be determined by Equation (2) [26]:

$$R_S = \frac{1}{n\mu e}. \quad (2)$$

where n is the sheet carrier concentration, μ is the carrier mobility, and e is per unit of charge.

As shown in Figure 3b, the sheet resistance first increases and then decreases with the increase in irradiation fluence. By Equation (2), this change is mainly due to the combined effect of proton irradiation on graphene sheet carrier concentration n and carrier mobility μ . The charge transfer between graphene and adsorbed gas can chemically dope the carbon nanostructures during irradiation, increasing the graphene channel's chemical doping and increasing the carrier concentration [27]. Due to the modulation of the graphene channel's sheet carrier concentration n by holes generated in the gate oxide [23,24], the sheet carrier concentration n gradually increases, and R_S gradually decreases during irradiation. However, due to the irradiation process, new impurities and defects are introduced into the graphene and graphene/gate oxide interfaces [28], resulting in enhanced Coulomb scattering, decreased carrier mobility μ , and a gradual increase in R_S . The change rule of the sheet resistance R_S is consistent with the changing trend of the carrier mobility μ , so it can be seen that the change in the electrical properties under proton irradiation is mainly affected by the carrier mobility.

Partial recovery of carrier mobility after irradiation at a fluence of 5×10^{11} p/cm² can be analyzed in reference [23,28,29]. The proton irradiation effect is a combined irradiation effect, so the results of studies with other radiation sources were used to explain this experiment. Graphene has a strong adsorption capacity for gases and impurities, which are inevitably adsorbed during the fabrication of graphene field-effect transistors. The Al₂O₃ layer in graphene field-effect transistors is so thin that gases can diffuse into the graphene. The analysis suggests that graphene channels before irradiation are less affected by gas adsorption because there are fewer graphene surface defects. After irradiation, the response of graphene to the adsorbed gases is more significant due to the increase in graphene surface states [23]. After irradiation, the absorption of atmospheric adsorbents and other impurities in the graphene channel and irradiation-induced defects are introduced into the graphene and graphene/gate oxide interfaces, and these dopants and defects act as scattering sites for carriers, leading to a decrease in carrier mobility and a decrease in the saturation current of the devices [28]. As the response of graphene to the adsorbed gas becomes larger during irradiation, the reaction of graphene-adsorbed O with graphene produces relatively low energy barriers for C–O and C=O. After irradiation at a fluence of 1×10^{11} p/cm², there will be a sizable number of vacancies on the surface, resulting in a sizable drop in carrier mobility. With the increase in proton fluence, the H concentration increases, which helps the desorption of O on graphene due to the tendency of H and O to form O–H, which not only reduces the scattering effect of adsorbed O on the carriers but also reduces the formation of vacancies during the reaction between O and graphene [29], leading to a partial restoration of the carrier mobility after irradiation with a fluence of 5×10^{11} p/cm².

3.2. TCAD Simulation of the Effect on the Electrical Characteristics for the Top-Gate GFETs Due to the Variation in the Graphene Channel Parameters

In this work, TCAD was used to simulate the effect of proton irradiation on top-gate GFETs. The result of varying the parameters of the graphene channel on the transfer characteristic curve was analyzed. The previous analysis shows that the effects of proton irradiation on top-gate GFETs are mainly carrier concentration and carrier mobility.

Figure 4 illustrates the cross-sectional structure at the channel of a top-gate GFET simulated using TCAD. The structure of the top-gate GFET is the same as that of a metal–oxide–semiconductor (MOS) transistor, except that the transistor channel is made of graphene material.

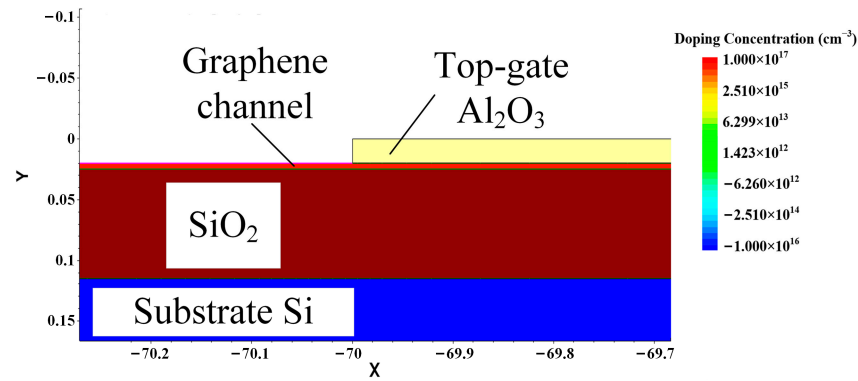


Figure 4. Schematic of the cross-section at the top-gate GFET channel based on TCAD simulation.

Reference [30] shows that the combination of the Philips Unified (PhuMob) Model and the high-field saturation model in the physical model provides the smoothest transfer characteristic curve. The addition of the Enormal mobility model would cause unwanted kinking effects at the Dirac point. Therefore, the PhuMob model and high-field saturation model were chosen as the moving models and SRH as the recombination model.

To better analyze the model of TCAD simulation, firstly, the fitting of the transfer characteristic curves of the simulated model to the actual test curves was carried out. The transfer characteristic curves of the top-gate GFETs simulated by TCAD were plotted against the experimental test curves, as shown in Figure 5. The transfer characteristic curve fitted by varying the graphene parameters matches the actual measured curve. This provides a theoretical basis for the subsequent analysis of the top-gate GFETs. Due to the difficulty of quantitative analysis with precise data, only relative values were used here to simulate different irradiation conditions.

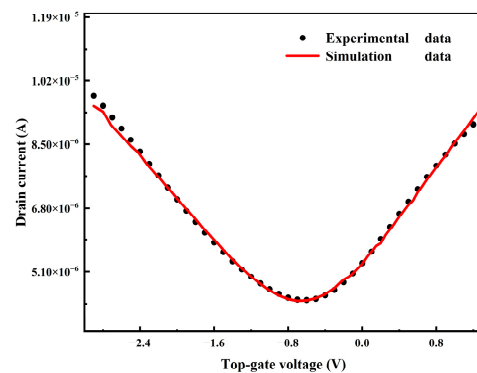


Figure 5. Plot of experimental data versus simulation data.

To analyze the effect of decreasing carrier mobility on the total current density of the device, we proceeded as follows: By varying the electron mobility and hole mobility in the graphene channel, the effect of different carrier mobility on the magnitude and distribution of the total current density in the channel was simulated, as shown in Figure 6. It can be seen that the decrease in mobility leads to an overall decrease in the total current density. The further away from the gate oxide, the lower the total current density.

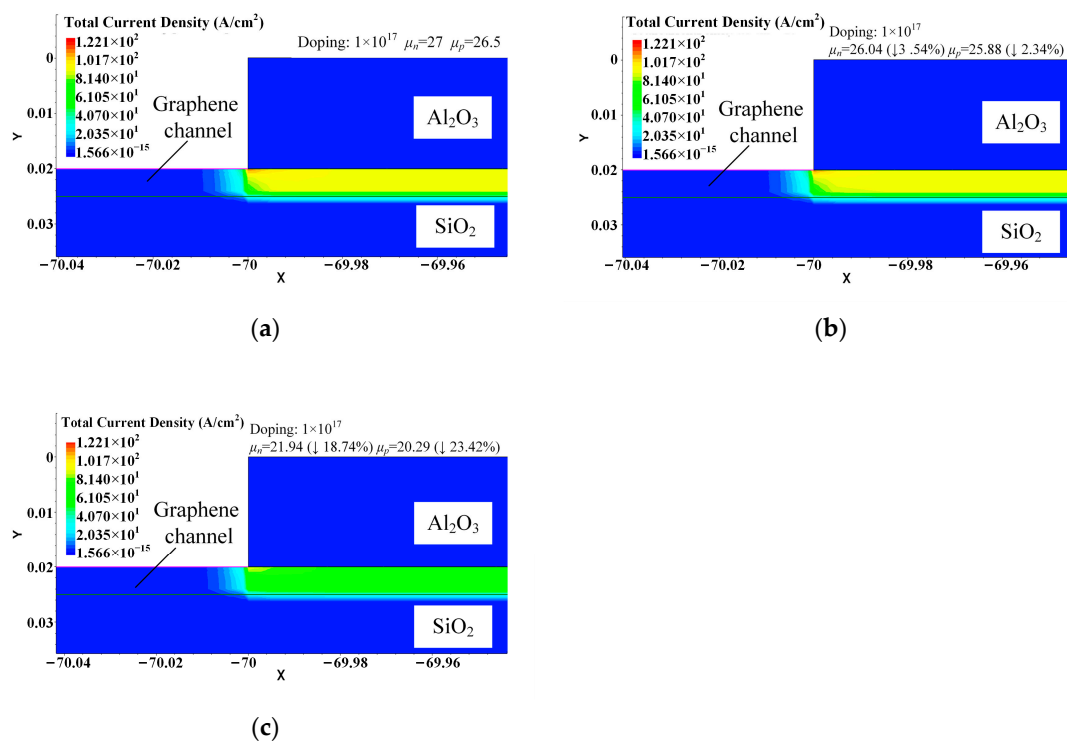


Figure 6. Total current density distribution at the channel for TCAD simulation. The N-type doping concentration is the same, and the carrier mobility is different. The ↓ in the figure represents the decrease, and the percentage represents the degree of decrease relative to the initial carrier mobility. (a) Electron mobility $\mu_n = 27$ and hole mobility $\mu_p = 26.5$. (b) Electron mobility $\mu_n = 26.04$ and hole mobility $\mu_p = 25.88$; reduction is consistent with the calculation. (c) Electron mobility $\mu_n = 21.94$ and hole mobility $\mu_p = 20.29$; reduction is consistent with the calculation.

To analyze the effect of increasing carrier concentration on the total current density of the device, we proceeded as follows: The simulation can change the carrier concentration by varying the doping concentration of the graphene channel. The effect of different carrier concentrations on the magnitude and distribution of the total current density in the channel was simulated by varying the doping in the graphene channel. As shown in Figure 7, the mobility is basically constant at a positive gate voltage.

As shown in Figure 8, the total current density at a negative gate voltage decreases with an increasing N-type doping concentration. When $V_{GS} = 0.5$ V, the device is dominated by electronic conduction at this point because this voltage point is to the right of the Dirac voltage point. When $V_{GS} = -2.5$ V, because this voltage point is to the left of the Dirac voltage point, the device is dominated by hole conduction. A comparison of Figures 7 and 8 shows that N-type doping has a more significant effect on the total current density when holes are the primary carriers.

To analyze the combined effect of carrier concentration and carrier mobility on the transfer characteristic curves of the top-gate GFETs, the combined effect on the transfer characteristic curves was analyzed by modifying the carrier mobility and carrier concentration of the graphene channel, as shown in Figure 9c. Because the Dirac voltage drifted negatively by 0.2 V after proton irradiation at all different fluences, the same doping concentration was used here. As shown in Figure 9c, the Dirac voltage of both devices negatively drifted from -0.6 V to -0.8 V after the increase in doping concentration, which is the same trend as the actual test. It can be seen that the simulated curves in Figure 9c are consistent with the trend of the test curves in Figure 3a. The black square curve in Figure 9c simulates the preirradiation situation and is also the simulated curve in Figure 5. The red dot curve simulates the 5×10^{11} p/cm² fluence case, and the green triangle curve simulates the 1×10^{11} p/cm² fluence case.

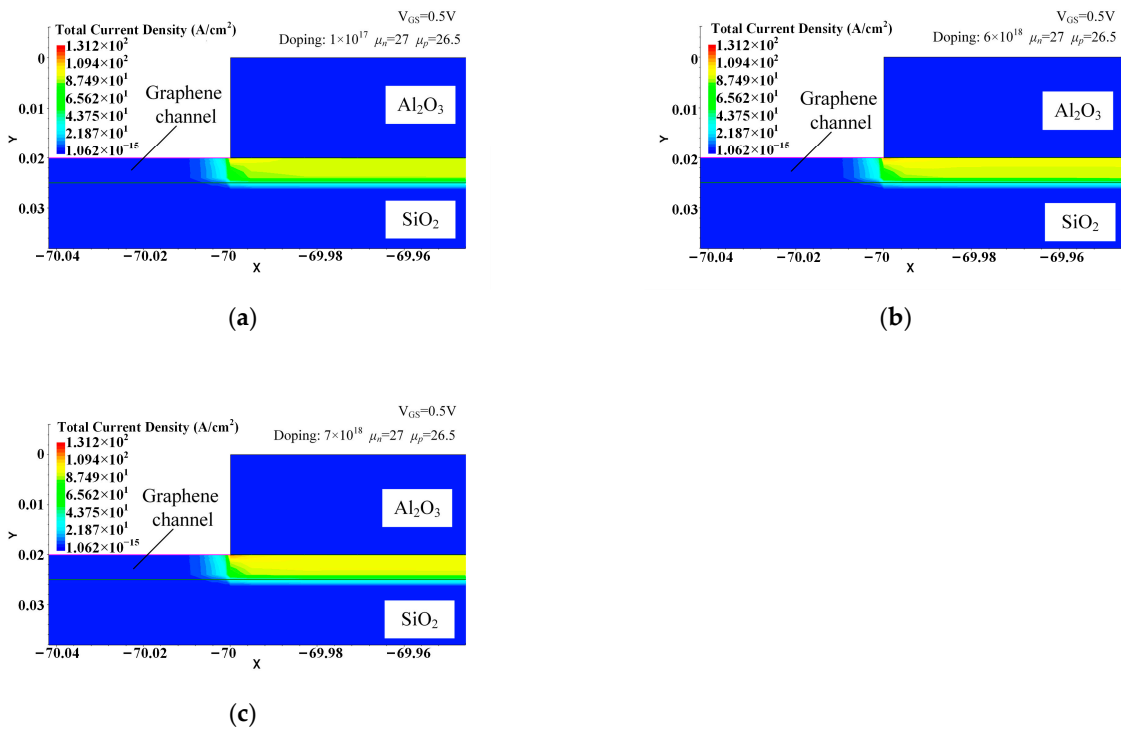


Figure 7. TCAD-simulated total channel current density distribution. The N-type doping concentration is different, and the carrier mobility is the same with $V_{GS} = 0.5$ V. (a) The N-type doping concentration is 1×10^{17} . (b) The N-type doping concentration is 6×10^{18} . (c) The N-type doping concentration is 7×10^{18} .

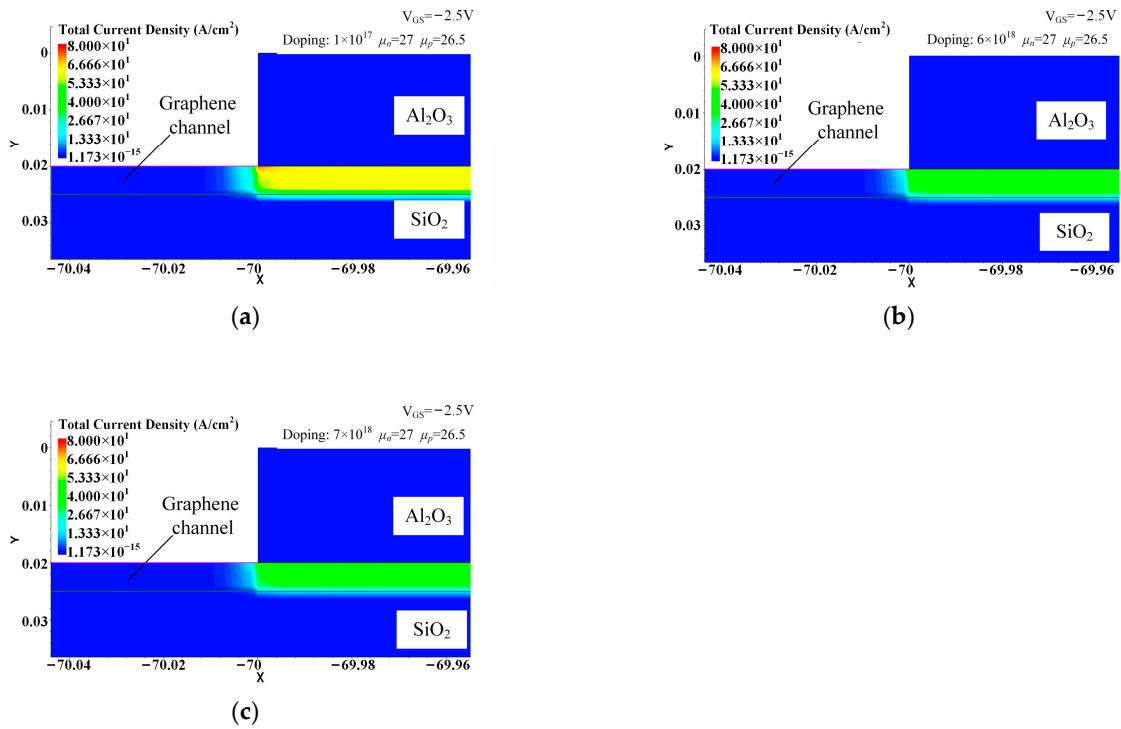


Figure 8. TCAD-simulated total channel current density distribution. The N-type doping concentration is different, and the carrier mobility is the same with $V_{GS} = -2.5$ V. (a) The N-type doping concentration is 1×10^{17} . (b) The N-type doping concentration is 6×10^{18} . (c) The N-type doping concentration is 7×10^{18} .

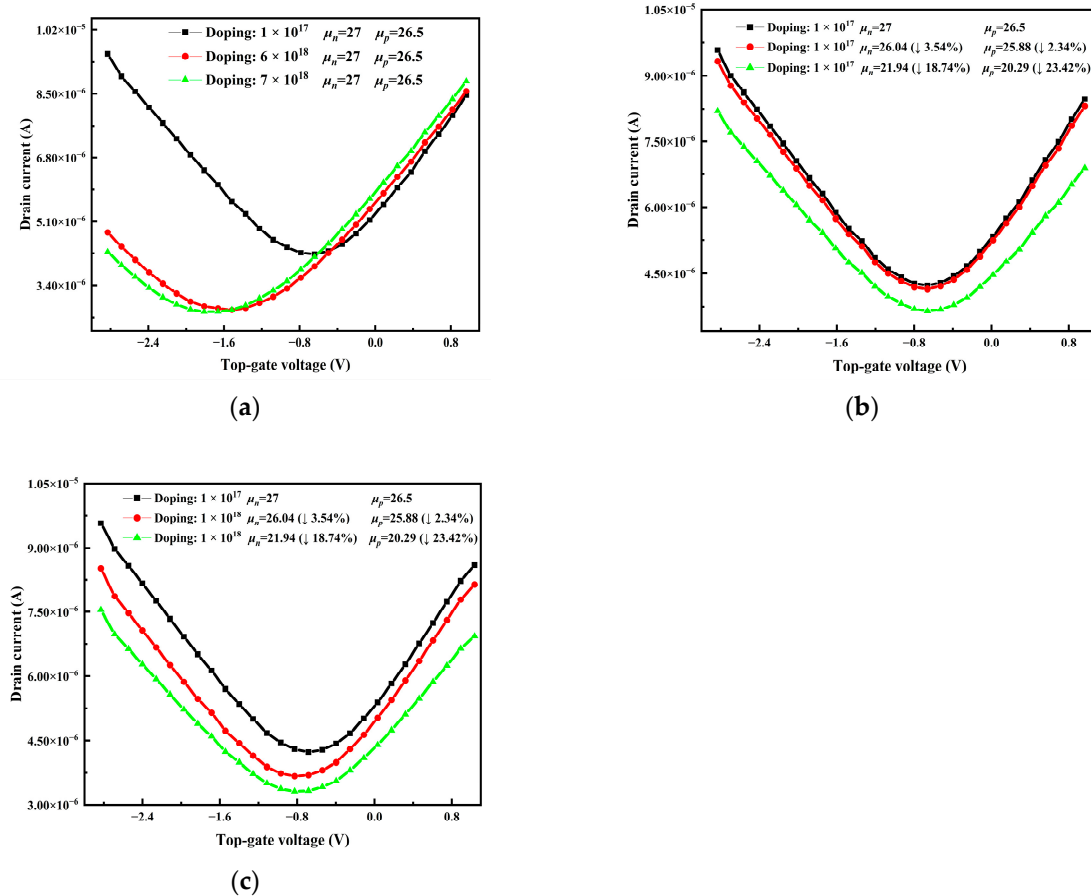


Figure 9. Transfer characteristic curves of top-gate GFETs simulated by TCAD. The \downarrow in the figure represents the decrease, and the percentage represents the degree of decrease relative to the initial carrier mobility. (a) Effect of different N-type doping concentrations for the same mobility. (b) Effect of different mobilities for the same N-type doping concentration. (c) The combined effect of different N-type doping concentrations and different carrier mobility.

As shown in Figure 9a, the degree of negative drift of the Dirac voltage increases with the increase in N-type doping concentration and gradually shifts from bipolar to N-type devices. As shown in Figure 9b, the change in carrier mobility does not drift the Dirac voltage, and the saturation current decreases with the decrease in carrier mobility. The results show that the increase in electron concentration in the graphene channel leads to a negative drift of the Dirac voltage, which is consistent with the previous analysis.

The effects of carrier concentration and mobility changes on the transfer characteristic curves were further analyzed, as shown in Figure 9c. On the one hand, the holes accumulated in the gate oxide layer during the irradiation process led to an increase in the electron concentration in the graphene channel, which gradually transformed the top-gate GFETs from a bipolar device to an N-type device, with a negative drift of the voltage at the Dirac point, an increase in the electron-dominated current on the right side of the Dirac, and a decay in the hole-dominated current on the left side of the Dirac. On the other hand, the change in carrier mobility due to the proton irradiation process similarly affects the electrical performance of the top-gate GFETs; i.e., as the carrier mobility decreases, the saturation current subsequently decays. According to Figure 9c, it is deduced that the decay of the saturation current is compatible with the reduction in carrier mobility. It can be shown that the changes in the electrical properties of the device following proton irradiation are dominated by carrier mobility.

3.3. Monte Carlo Simulation of Ionizing and Nonionizing Energy Losses Produced by Proton Irradiation in Top-Gate GFETs

In this article, the Monte Carlo simulation and modeling software SRIM 2008 [31,32] was further used to simulate the physical processes of particle motion in matter.

SRIM simulation requires first determining the device structure and the materials, densities, and thicknesses used for each structure. The thickness of Al_2O_3 used in the device was EOT (equivalent oxide thickness) 20 nm, which can be converted to the actual thickness by Equation (3) [33]:

$$\frac{t_{\text{ox}}}{\epsilon_{\text{ox}}} = \frac{t_{\text{high-k}}}{\epsilon_{\text{high-k}}} \quad (3)$$

where t_{ox} and ϵ_{ox} are the thickness and dielectric constant of SiO_2 , respectively, and $t_{\text{high-k}}$ and $\epsilon_{\text{high-k}}$ are the thickness and dielectric constant of the higher k-gate dielectric, respectively; the thickness of Al_2O_3 was calculated to be 512.8 Å, the theoretical thickness of graphene to be 3.35 Å [34], and the thickness of SiO_2 to be 900 Å. The thickness of the silicon substrate was taken to be only 2000 Å because the main study was the energy loss near the graphene channel.

To minimize the simulation error, a sufficiently large sample needed to be selected for the simulation. In this calculation, 10^5 of 20 MeV protons, which are incident vertically from the center of the target surface, were used. To better understand the equivalent TID levels for this proton irradiation experiment, the TID levels could be equivalently converted via Equation (4) [35]:

$$\text{TID} = 1.6 \times 10^{-5} \times \text{LET} \times \text{Proton Fluence} \quad (4)$$

The SRIM simulations show the LET value of 0.0203 MeVcm²/mg at the proton energy of 20 MeV. The total ionizing dose (TID) is 32.48 krad(Si) and 162.4 krad(Si) for fluences of up to 1×10^{11} p/cm² and 5×10^{11} p/cm², respectively.

As shown in Figure 10, the particle trajectory diagram of a 20 MeV proton in a top-gate GFET device is simulated. It can be seen that the particles have only a few collisions in the Al_2O_3 and SiO_2 layers, and most of the particles can pass right through this region. The energy loss from this collision is also reflected in the nonionization energy loss in Figure 11.

The energy loss due to 20 MeV proton irradiation of the top-gate GFET device was categorized into ionization and nonionization energy losses. Simulations were performed using SRIM to understand the magnitude and distribution of these two types of energy losses in top-gate GFET devices. The variation in ionization energy loss and nonionizing energy loss induced by proton irradiation of a top-gate GFET device with the depth of the device was simulated, as shown in Figure 11.

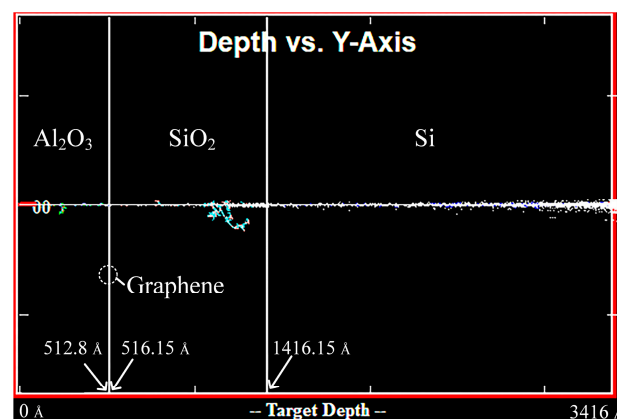


Figure 10. Particle trajectory diagram of a 20 MeV proton in a top-gate GFET device.

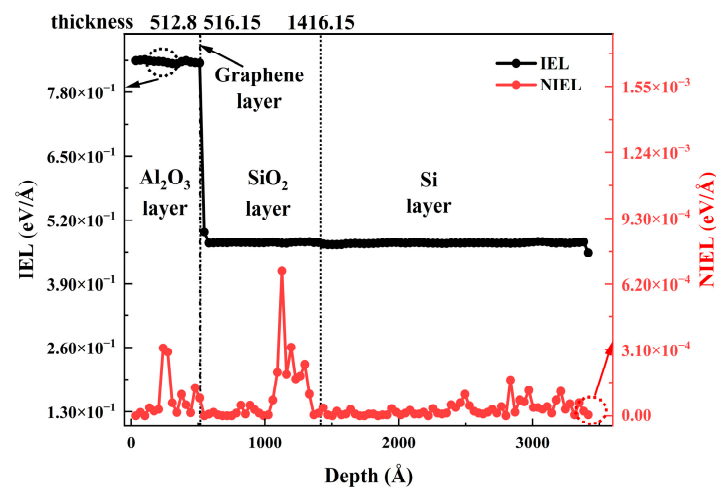


Figure 11. SRIM-simulated ionization energy loss and nonionizing energy loss with a depth of 20 MeV protons in the top-gate GFETs.

The SRIM simulation results show that the ionization energy loss of 20 MeV protons in top-gate GFET devices is mainly concentrated at the Al_2O_3 (gate oxide) and graphene/gate oxide interfaces. The ionization energy loss is two or even three orders of magnitude higher than the nonionization energy loss at the same depth. Therefore, it can be assumed that the energy loss produced by 20 MeV proton irradiation in top-gate GFET devices is mainly an ionization energy loss and is concentrated at the gate oxide and graphene/gate oxide interfaces. The oxide trap charge due to ionization damage and the interface state trap charge due to irradiation-generated defects significantly impact top-gate GFETs and their performance.

4. Conclusions

In this article, the high-energy proton irradiation effect was investigated for top-gate GFETs. The experimental results show that irradiation leads to a negative voltage drift and an increase in sheet resistance at the Dirac point, a saturation current decay, and a decrease in the hole mobility and electron mobility of the top-gate GFETs. The partial recovery of mobility for a fluence of 5×10^{11} p/cm² compared to 1×10^{11} p/cm² can be attributed to the H-promoted desorption of O, which reduces the adsorption of O and the formation of vacancies during the reaction of O with graphene. The negative drift of the Dirac point voltage is attributed to the ionization effect of proton irradiation on the gate oxide, which modulates the gate electric field. The increase in sheet resistance and the attenuation of the saturation current are mainly due to the decrease in carrier mobility of the graphene channel as a function of proton irradiation. After 33 days of room-temperature annealing, the saturation current and the Dirac voltage of the device were partially recovered, and the Dirac sheet resistance increased. The effects of changes in carrier concentration and mobility of graphene channels on the transfer characteristic curves of top-gate GFETs, in which carrier mobility plays a primary role, were verified by TCAD simulations. Through Monte Carlo simulations, it was obtained that the ionization energy loss induced by proton irradiation within the device was mainly concentrated at the gate oxide and graphene/gate oxide interfaces, which also indicates that the effect of proton irradiation on the gate oxide and graphene/gate oxide interfaces of the top-gate GFETs cannot be neglected. This study illustrates that 20 MeV proton irradiation has a significant effect on the electrical performance of top-gate GFETs, and the energy loss and distribution shown by simulation provide a basis for the radiation hardened of the device.

Author Contributions: Conceptualization, X.L., H.G., Z.L. and X.Z.; methodology, X.L.; software, X.L.; validation, X.L., J.L. and W.M.; formal analysis, X.L.; investigation, X.L.; resources, X.L.; data curation, X.L.; writing—original draft preparation, X.L.; writing—review and editing, X.L., C.P., H.Z., Y.F., T.M. and Z.Z.; visualization, X.L., Y.L. and R.B.; supervision, H.G.; project administration, H.G.; funding acquisition, H.G., Z.L. and X.Z. All authors have read and agreed to the published version of the manuscript.

Funding: This work was supported by the National Natural Science Foundation of China (Nos. 12275230, 12027813, and 12305299), the Foundation of National Key Laboratory of Materials Behavior and Evaluation Technology in Space Environment (No. 6142910220209), and GuangDong Basic and Applied Basic Research Foundation (No. 2022A1515111049).

Institutional Review Board Statement: Not applicable.

Informed Consent Statement: Not applicable.

Data Availability Statement: The data presented in this study are available in this article.

Conflicts of Interest: The authors declare no conflict of interest.

References

1. Park, B.; Ho, D.; Kwon, G.; Kim, D.; Seo, S.Y.; Kim, C.; Kim, M. Solution-Processed Rad-Hard Amorphous Metal-Oxide Thin-Film Transistors. *Adv. Funct. Mater.* **2018**, *28*, 1802717. [[CrossRef](#)]
2. Basiricò, L.; Basile, A.F.; Cosseddu, P.; Gerardin, S.; Cramer, T.; Bagatin, M.; Ciavatti, A.; Paccagnella, A.; Bonfiglio, A.; Fraboni, B. Space Environment Effects on Flexible, Low-Voltage Organic Thin-Film Transistors. *ACS Appl. Mater. Interfaces* **2017**, *9*, 35150–35158. [[CrossRef](#)]
3. Ho, D.; Choi, S.; Kang, H.; Park, B.; Le, M.N.; Park, S.K.; Kim, M.-G.; Kim, C.; Facchetti, A. In Situ Radiation Hardness Study of Amorphous Zn–In–Sn–O Thin-Film Transistors with Structural Plasticity and Defect Tolerance. *ACS Appl. Mater. Interfaces* **2023**, *15*, 33751–33762. [[CrossRef](#)]
4. Novoselov, K.S.; Geim, A.K.; Morozov, S.V.; Jiang, D.; Zhang, Y.; Dubonos, S.V.; Grigorieva, I.V.; Firsov, A.A. Electric Field Effect in Atomically Thin Carbon Films. *Science* **2004**, *306*, 666–669. [[CrossRef](#)]
5. Novoselov, K.S.; Geim, A.K.; Morozov, S.V.; Jiang, D.; Katsnelson, M.I.; Grigorieva, I.V.; Dubonos, S.V.; Firsov, A.A. Two-Dimensional Gas of Massless Dirac Fermions in Graphene. *Nature* **2005**, *438*, 197–200. [[CrossRef](#)] [[PubMed](#)]
6. Bolotin, K.I.; Sikes, K.J.; Jiang, Z.; Klima, M.; Fudenberg, G.; Hone, J.; Kim, P.; Stormer, H.L. Ultrahigh Electron Mobility in Suspended Graphene. *Solid State Commun.* **2008**, *146*, 351–355. [[CrossRef](#)]
7. Balandin, A.A.; Ghosh, S.; Bao, W.; Calizo, I.; Teweldebrhan, D.; Miao, F.; Lau, C.N. Superior Thermal Conductivity of Single-Layer Graphene. *Nano Lett.* **2008**, *8*, 902–907. [[CrossRef](#)] [[PubMed](#)]
8. Lee, C.; Wei, X.; Kysar, J.W.; Hone, J. Measurement of the Elastic Properties and Intrinsic Strength of Monolayer Graphene. *Science* **2008**, *321*, 385–388. [[CrossRef](#)]
9. Kumar, S.; Tripathi, A.; Khan, S.A.; Pannu, C.; Avasthi, D.K. Radiation Stability of Graphene under Extreme Conditions. *Appl. Phys. Lett.* **2014**, *105*, 133107. [[CrossRef](#)]
10. Ji, Q.; Liu, J.; Yang, M.; Hu, X.; Wang, G.; Qiu, M.; Liu, S. Influence of Proton Irradiation Energy on Gate–Channel Low-Field Electron Mobility in AlGaIn/GaN HEMTs. *Electronics* **2023**, *12*, 1473. [[CrossRef](#)]
11. Wang, P.F.; Zhang, E.X.; Chuang, K.H.; Liao, W.; Gong, H.; Wang, P.; Arutt, C.N.; Ni, K.; Mccurdy, M.W.; Verbauwhede, I.; et al. X-ray and Proton Radiation Effects on 40 Nm CMOS Physically Unclonable Function Devices. *IEEE Trans. Nucl. Sci.* **2018**, *65*, 1519–1524. [[CrossRef](#)]
12. Ristić, G.S.; Andjelković, M.; Savović, S. The Isochronal Annealing of Irradiated N-Channel Power VDMOSFETs. *Nucl. Instrum. Methods Phys. Res. Sect. B Beam Interact. Mater. At.* **2016**, *366*, 171–178. [[CrossRef](#)]
13. Ko, G.; Kim, H.-Y.; Ren, F.; Pearton, S.J.; Kim, J. Electrical Characterization of 5 MeV Proton-Irradiated Few Layer Graphene. *Electrochem. Solid-State Lett.* **2010**, *13*, K32. [[CrossRef](#)]
14. Yang, G.; Kim, B.-J.; Kim, K.; Han, J.W.; Kim, J. Energy and Dose Dependence of Proton-Irradiation Damage in Graphene. *RSC Adv.* **2015**, *5*, 31861–31865. [[CrossRef](#)]
15. Cui, N.; Liu, Y.; Jiang, H.; Guo, J. Obvious Difference between Protons and Electrons Irradiation on the Performance of Graphene Devices. *Int. J. Mod. Phys. B* **2023**, *37*, 2350205. [[CrossRef](#)]
16. Francis, S.A.; Petrosky, J.C.; McClory, J.W.; Cress, C.D. Effects of Proton and X-ray Irradiation on Graphene Field-Effect Transistors with Thin Gate Dielectrics. *IEEE Trans. Nucl. Sci.* **2014**, *61*, 3010–3017. [[CrossRef](#)]
17. Zhang, Y.; Peng, S.; Wang, Y.; Guo, L.; Zhang, X.; Huang, H.; Su, S.; Wang, X.; Xue, J. Environment-Dependent Radiation Tolerance of Graphene Transistors under Proton Irradiation. *J. Phys. Chem. Lett.* **2022**, *13*, 10722–10727. [[CrossRef](#)]
18. Fan, L.; Bi, J.; Xi, K.; Yang, X.; Xu, Y.; Ji, L. Impact of γ -Ray Irradiation on Graphene-Based Hall Sensors. *IEEE Sens. J.* **2021**, *21*, 16100–16106. [[CrossRef](#)]

19. Efil Kutluoğlu, E.; Öz Orhan, E.; Bayram, Ö.; Bilge Ocak, S. Gamma-Ray Irradiation Effects on Capacitance and Conductance of Graphene-Based Schottky Diode. *Phys. B Condens. Matter* **2021**, *621*, 413306. [CrossRef]
20. Lee, S.; Seo, J.; Hong, J.; Park, S.H.; Lee, J.-H.; Min, B.-W.; Lee, T. Proton Irradiation Energy Dependence of Defect Formation in Graphene. *Appl. Surf. Sci.* **2015**, *344*, 52–56. [CrossRef]
21. Graphenea, GFET-S31. Available online: <https://www.graphenea.com> (accessed on 19 March 2023).
22. Schwierz, F. Graphene Transistors. *Nat. Nanotechnol.* **2010**, *5*, 487–496. [CrossRef] [PubMed]
23. Lu, G.; Ocola, L.E.; Chen, J. Gas Detection Using Low-Temperature Reduced Graphene Oxide Sheets. *Appl. Phys. Lett.* **2009**, *94*, 083111. [CrossRef]
24. Fowler, J.D.; Allen, M.J.; Tung, V.C.; Yang, Y.; Kaner, R.B.; Weiller, B.H. Practical Chemical Sensors from Chemically Derived Graphene. *ACS Nano* **2009**, *3*, 301–306. [CrossRef] [PubMed]
25. Liang, X.; Fu, Z.; Chou, S.Y. Graphene Transistors Fabricated via Transfer-Printing in Device Active-Areas on Large Wafer. *Nano Lett.* **2007**, *7*, 3840–3844. [CrossRef]
26. Liu, E.; Zhu, B.; Luo, J. *The Physics of Semiconductors*, 7th ed.; Publishing House of Electronics Industry: Beijing, China, 2011; pp. 123–125.
27. Schedin, F.; Geim, A.K.; Morozov, S.V.; Hill, E.W.; Blake, P.; Katsnelson, M.I.; Novoselov, K.S. Detection of Individual Gas Molecules Adsorbed on Graphene. *Nat. Mater.* **2007**, *6*, 652–655. [CrossRef] [PubMed]
28. Jain, S.; Gajarushi, A.S.; Gupta, A.; Rao, V.R. A Passive Gamma Radiation Dosimeter Using Graphene Field Effect Transistor. *IEEE Sens. J.* **2020**, *20*, 2938–2944. [CrossRef]
29. Puzyrev, Y.S.; Wang, B.; Zhang, E.X.; Zhang, C.X.; Newaz, A.K.M.; Bolotin, K.I.; Fleetwood, D.M.; Schrimpf, R.D.; Pantelides, S.T. Surface Reactions and Defect Formation in Irradiated Graphene Devices. *IEEE Trans. Nucl. Sci.* **2012**, *59*, 3039–3044. [CrossRef]
30. Ismail, M.A.; Zaini, K.M.M.; Syono, M.I. Graphene Field-Effect Transistor Simulation with TCAD on Top-Gate Dielectric Influences. *TELKOMNIKA Telecommun. Comput. Electron. Control* **2019**, *17*, 1845. [CrossRef]
31. Ziegler, J.F. SRIM-2003. *Nucl. Instrum. Methods Phys. Res. Sect. B Beam Interact. Mater. At.* **2004**, *219–220*, 1027–1036. [CrossRef]
32. Ziegler, J.F.; Ziegler, M.D.; Biersack, J.P. SRIM—The Stopping and Range of Ions in Matter (2010). *Nucl. Instrum. Methods Phys. Res. Sect. B Beam Interact. Mater. At.* **2010**, *268*, 1818–1823. [CrossRef]
33. Chen, S.; Wang, W.; Cai, X.; Chen, D.; Wang, X.; Han, X. The Technology of EOT Control in High k Dielectric/Metal Gate Electrode CMOS Device. *Equip. Electron. Prod. Manuf.* **2010**, *3*, 11–16. [CrossRef]
34. Wang, W.; Wang, S.; Zhang, S.; Wang, W.; Ji, X.; Li, C. Effects of Substrates on Proton Irradiation Damage of Graphene. *RSC Adv.* **2020**, *10*, 12060–12067. [CrossRef] [PubMed]
35. Bai, R.-X.; Guo, H.-X.; Zhang, H.; Wang, D.; Zhang, F.-Q.; Pan, X.-Y.; Ma, W.-Y.; Hu, J.-W.; Liu, Y.-W.; Yang, Y.; et al. High-Energy Proton Radiation Effect of Gallium Nitride Power Device with Enhanced Cascode Structure. *Acta Phys. Sin.* **2023**, *72*, 012401. [CrossRef]

Disclaimer/Publisher’s Note: The statements, opinions and data contained in all publications are solely those of the individual author(s) and contributor(s) and not of MDPI and/or the editor(s). MDPI and/or the editor(s) disclaim responsibility for any injury to people or property resulting from any ideas, methods, instructions or products referred to in the content.